Available online at www.sciencedirect.com
SCIENCE DIRECT®
Journal of Electron Spectroscopy and Related Phenomena 144–147 (2005) 1151–1155
JOURNAL OF ELECTRON SPECTROSCOPY and Related Phenomena
www.elsevier.com/locate/elspec

A novel-type tunable and narrowband extreme ultraviolet radiation source based on high-harmonic conversion of picosecond laser pulses

M. Barkauskas[a], F. Brandi[a], F. Giammanco[b], D. Neshev[c,*], A. Pirri[a], W. Ubachs[a]

[a] *Laser Centre, Department of Physics and Astronomy, Vrije Universiteit, De Boelelaan 1081, 1081 HV Amsterdam, The Netherlands*
[b] *Department of Physics, University of Pisa, Via F. Buonarotti 2, 56127 Pisa, Italy*
[c] *Nonlinear Physics Centre, Research School of Physical Sciences and Engineering, Australian National University, Canberra, Australia*

Available online 26 February 2005

Abstract

At the Laser Centre Vrije Universiteit a table-top size, tunable and narrowband laser-based source of extreme ultraviolet radiation was developed using high-harmonic generation of powerful laser pulses of 300 ps duration and Fourier-transform limited bandwidth. The generated radiation has unprecedented spectral purity of $\lambda/\Delta\lambda > 2.5 \times 10^5$ at wavelengths covering the entire tunability range of 40–100 nm. The process of high-order harmonic generation was investigated in different gases (Ar, Kr, Xe, N_2) uncovering resonance phenomena for the conversion efficiency of specific harmonic orders.

Keywords: Extreme ultraviolet radiation; High-harmonic generation; Laser spectroscopy

1. Introduction

The generation of high-order harmonics by atoms exposed to intense laser fields has been pursued in the recent decade with the goal of extending sources of coherent radiation to the vacuum ultraviolet (VUV) and extreme ultraviolet (XUV) part of the electromagnetic spectrum. The majority of high-order harmonic generation (HHG) experiments are performed with mode-locked lasers delivering short pulses (from 5 fs to 50 ps), thus allowing to reach intensities above 10^{13} W/cm^2, required to generate harmonics in the non-perturbative regime. Employing modern femtosecond lasers, with peak intensities in the focus up to $\sim 10^{16}$ W/cm^2, harmonics of order ~400 can be readily generated [1]. Although in this case, the structure of harmonics is lost and the source exhibits a "white" spectrum, coherent radiation in and beyond the so called "water window" is produced [2]. These systems have many applications in various fields of science, especially in time resolved spectroscopy, attophysics, as well as in biological studies [3], but they are inherently unsuitable for high-precision frequency-domain spectroscopy in the XUV due to their broadband spectrum.

Nanosecond pulsed lasers have a superior spectral performance, but to reach intensities of 10^{13} W/cm^2 with a reasonably sized Q-switched ns laser is cumbersome. Even if achieved, such long and highly energetic pulses will fully ionize the gaseous nonlinear medium on the rising edge of the pulse, thus prohibiting neutral atoms to be exposed to the peak intensity. Although Eikema et al. [4] succeeded in generating the fifth harmonic at wavelengths as short as 58 nm with Fourier-transform limited nanosecond pulses, further increase of the pulse energies, in order to increase conversion efficiencies of generated harmonics or to generate radiation at even shorter wavelengths, is hardly feasible. An alternative strategy to generate short wavelengths was pursued by Rupper and Merkt [5] by incorporating the powerful VUV-output of an F_2-excimer laser at 157 nm in a low-order wave-mixing scheme. A different, tunable wavelength source of XUV radiation for time and frequency domain spectroscopy, based on HHG, was built in Lund, employing pulses of ~50 ps duration and obtaining a spectral purity of $\sim 10^4$ [6].

Here, we present a novel tunable, HHG based XUV source with an improved spectral purity of $\lambda/\Delta\lambda > 2.5 \times 10^5$ at the

* Corresponding author.
E-mail address: dragomir.neshev@anu.edu.au (D. Neshev).

0368-2048/$ – see front matter © 2005 Elsevier B.V. All rights reserved.
doi:10.1016/j.elspec.2005.01.208

cost of a longer pulse duration (300 ps). Aspects of the harmonic conversion process and XUV-yield have been reported earlier [7] and in this work, we present detail analysis on the conversion in a number of gases and resonance behavior at some harmonic frequencies and wavelengths.

2. Setup

A detailed description of the laser system was reported in Ref. [8]. A schematic diagram of the experimental setup is shown in Fig. 1. This table-top XUV–laser system, fitting on to a single optical table is built from five sub-units shown in dashed boxes.

The first stage is a narrow-band seeder, where the seeding light is produced by a tunable cw Ti:Sapphire laser (Microlase Optical Systems MBR-110) which is pumped by a Millennia-V (Spectra Physics) laser. The Ti:Sapphire ring laser can be tuned through its entire gain curve (700–970 nm) and is operated at a bandwidth of several MHz. Continuous tuning is possible over 40 GHz. The wavelength of this seed-laser determines the frequency of the amplified pulses and correspondingly the XUV harmonic-output.

A single injection seeded, Q-switched Nd:YAG (Quanta Ray GCR-330) laser operating at 10 Hz repetition rate is used for pumping the Ti:Sapphire amplifiers and the stimulated Brillouin scattering (SBS) pulse compressor. The latter consists of a 1 m long water cell and delivers FT-limited pulses of 300 ps duration at 532 nm as described in detail in Ref. [9].

The cw output of the seed-laser is converted into pulses in a three-stage travelling-wave pulsed dye amplifier (PDA), thus providing pulses of 1 mJ energy and 300 ps duration. The present measurements were performed operating LDS 765 dye (Exciton). The amplification bandwidth of a typical dye is ∼50 nm; thus, in order for the laser system to cover the whole Ti:Sapphire gain spectrum, dyes need to be changed.

Further amplification of the pulses is accomplished in a single-pass Ti:Sapphire preamplifier and a multi-pass Ti:Sapphire amplifier. The pump energy (1 J, at 532 nm, 5 ns) is divided by a 90/10 beam splitter, where the smaller portion pumps the preamplifier and the rest is divided once more by a 50/50 beam splitter and, after mild focusing, pumps the main four-pass amplifier from two sides. The Ti:Sapphire crystal in the amplifier is cylindrically shaped with diameter and length of 10 mm and water cooled. Finally near-infrared (NIR) pulses of 220 mJ energy and 300 ps duration are produced at a 10 Hz repetition rate with tunability in the range 750–795 nm (with decrease of pulse energy at the edges of this range).

The NIR output pulses have a bandwidth of 1.5 GHz [8] and a time-bandwidth product of $\Delta\tau \times \Delta\nu = 0.45$, demonstrating that the powerful infrared pulses are FT-limited. The laser beam was focused by a 20 cm lens and the intensity in the waist was estimated to be 5.1×10^{13} W/cm^2 (assuming 200 mJ pulses). This intensity is sufficient to perform HHG in the so-called plateau region.

Harmonics are produced in a vacuum system consisting of three differentially pumped chambers. The NIR pulses are focused in a freely expanding gas jet, typically 1 mm under the orifice of a piezo-electric nozzle. A normal incidence spherical grating (1 m focal distance) separates the generated harmonics and refocuses them onto a slit. The selected harmonics are than detected with an electron multiplier tube (EMT). The third vacuum chamber is equipped with a pulsed valve to inject a probe gas for the purpose of performing absorption experiments in a gas jet.

3. Results

A typical high-harmonic spectrum is presented in the inset of Fig. 1. All the measurements presented here, are performed with 2 bar gas backing pressure, which is estimated to correspond to a density of $(3–10)\times10^{17}$ particles/cm^3 in the interaction region. The number of photons generated in the harmonics is estimated, by taking into account the grating re-

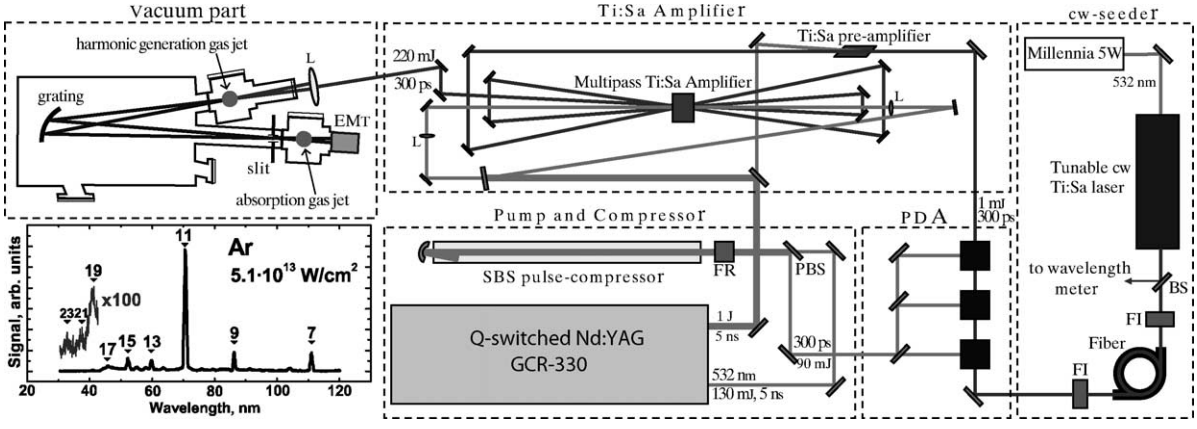

Fig. 1. Schematic diagram of the experimental setup: BS, beam splitter; FI, Faraday isolator; PBS, polarizing beam splitter; FR, Fresnel Rhomb; L, lens; EMT, Electron multiplier tube. Insert in the left bottom corner: EMT signal performing a typical scan by rotating the grating. Note that relative intensity of high-harmonics needs to be rescaled for grating reflectivity and EMT quantum efficiency. See text for further description.

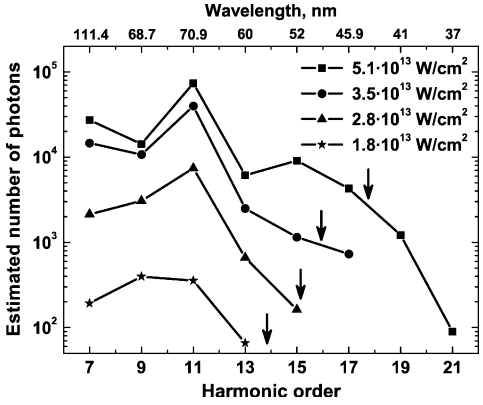

Fig. 2. High-harmonics generated in Ar for different intensities at $\lambda =$ 780 nm (vertical axis: estimated number of photons per pulse). Arrow indicates calculated cut-off position for different intensities (formula from Ref. [12] was used).

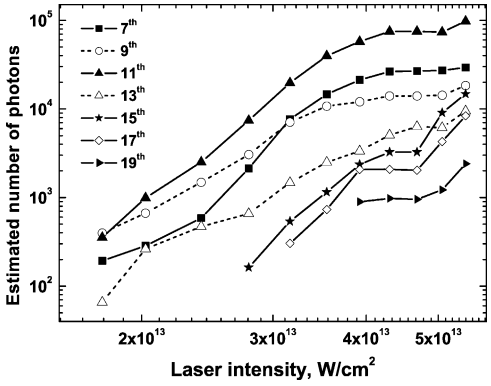

Fig. 3. Log–log plot of harmonic yield generated in Ar vs. laser intensity. Fundamental wavelength 780 nm. The slopes at lower intensities for the 7th and 11th harmonics are ∼ 7 and for 9th and 13th ∼5.

flectivity for the first diffraction order, the quantum efficiency of the first dynode (BeCu) of the EMT and the detector gain as specified by the manufacturers. The results for various input intensities are presented in Fig. 2. The estimated absolute number of photons should be taken with some precaution, because of possible degrading of the grating and decrease of the EMT performance with time. The grating in use is gold-coated and therefore has a cutoff for reflection below 40 nm.

In Fig. 2, the main features of HHG can be seen: the plateau-like behavior of harmonics followed by a sudden cut-off. The cut-off law, determining the highest order harmonic, N_{max}, is given by [13]:

$$N_{max} = \frac{I_p + 3U_p}{\omega}, \quad (1)$$

where I_p is the ionization potential and U_p (eV) $= 9.33 \times 10^{-14} I$ (W/cm^2)λ^2 (μm) the ponderomotive potential, that is, the mean kinetic energy acquired by an electron oscillating in the laser field. I and λ are the laser intensity and wavelength, respectively. Minor corrections were introduced to this formula by a fully quantum mechanical description of the process of HHG [12]. At the highest intensity of 5.1×10^{13} W/cm^2, indeed, a cut-off is found in between the 17th and 19th order, as predicted. For lower intensities, the cut-off region is not reached, which is interpreted as the intensity being too low for reaching the non-perturbative regime, where harmonic generation is described by a three step model [11,12]. This model describes semiclassically the HHG process as: excitation of an electron to the continuum by photo-ionization of the atom, followed by acceleration of the free electron in the strong laser field and finally recombination with the parent ion and emission of a harmonic photon.

In Fig. 3, the harmonic yield is plotted versus intensity to visualize saturation effects. At lower intensities, the conversion efficiencies follow a power law, which levels off at higher intensities. The saturation point, represented by intensity I_s, can be qualitatively defined as the intensity at which the probability for an atom to be ionized approaches one. Quantitatively, I_s is the intensity for which the growth in the ion–yield curve levels off to a $\frac{3}{2}$ power law [10]. Obviously, I_s decreases with increase of the pulse duration τ, specifically, $I_s \propto \tau^{-1/n}$, where n is the minimum number of photons necessary to ionize the atom; thus, for our relatively long pulses (300 ps) it is reached at low intensities. To evaluate the degree of ionization, measurements of the ion yield for different gases were performed as a function of the input intensity (see Fig. 4). Ions are collected by a metallic grid, with negative potential, placed underneath the harmonic generation gas jet. Results shown in Fig. 4 indicate that the saturation intensity for Ar is at $I_s^{exp} \sim 4.5 \times 10^{13}$ W/cm^2. This is in good agreement with the theoretically calculated value of I_s^{cal}(Ar) $= 4.9 \times 10^{13}$ W/cm^2 for 300 ps pulses [10]. The observed correlation (Figs. 3 and 4 for Ar) between high-order harmonic yield and ionization of the medium is predicted by the three step model of HHG. Thus the nearly constant high-harmonic yield is caused by saturation of ionization.

Exploiting the wavelength tunability of the system we performed investigation of the harmonic yield dependencies on the wavelength for various generating gases (Ar, N_2 and Kr shown in Figs. 5–7, respectively). A resonance-like

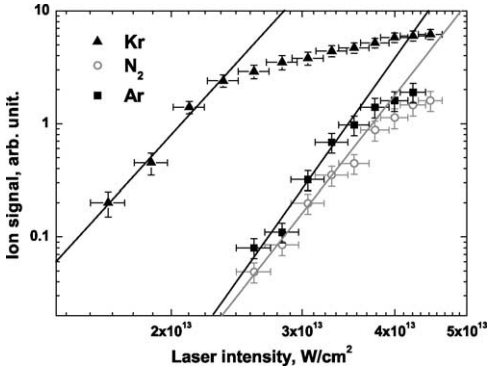

Fig. 4. Log–log plot of ionization vs. intensity for different gases. Fundamental wavelength 780 nm. The slopes at lower intensities are: Ar, 9.3 ± 1.4; N_2, 8.4 ± 0.5; Kr, 7.3 ± 0.5.

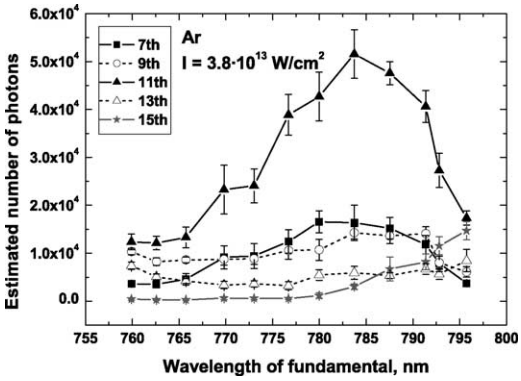

Fig. 5. Harmonic yield dependence on fundamental wavelength for Ar. Laser intensity in the focus was kept constant 3.8×10^{13} W/cm^2.

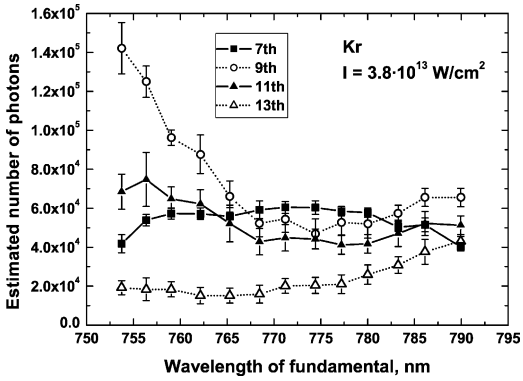

Fig. 7. Harmonic yield dependence on fundamental wavelength for Kr. Laser intensity in the focus was kept constant 3.8×10^{13} W/cm^2.

phenomenon is apparent for the 11th harmonic generated in Ar with wavelengths of the fundamental in the 770–795 nm range (Fig. 5). This explains also why in Fig. 2 (taken at 780 nm) the 11th harmonic is more efficient than other harmonics on the plateau; qualitatively similar behavior is observed for the 7th harmonic but not for the 9th and 13th. The difference between these harmonic pairs is also evident in Fig. 3, where they follow different intensity power laws leading to saturation. Similar resonance-like behavior is observed for the 9th harmonic in N_2 and Kr (Figs. 6 and 7).

A quantitative explanation for this resonance behavior in HHG is still under investigation; however, two physical phenomena can be identified to cause such effects. First, phase-matching conditions at some combinations of harmonic order and wavelength may lead to optimum conversion, and secondly the quantized level structure of the species used may exhibit multi-photon resonances to increase HHG-yield. Further studies may reveal whether a collective or a single-atom effect lies at the origin of the resonances.

Ar and N_2 have similar ionization potentials (15.76 and 15.58 eV, respectively), thus making the ionization dynamics alike as confirmed by ionization measurements in Fig. 4. Hence, the temporal and spatial free-electron contributions to the refractive index n are similar. In the optical region, $n_{Ar} = 1.000281$ and $n_{N_2} = 1.000298$ (at 273 K, 1 atm and 589.3 nm), and assuming n close to 1 for both gases in the XUV, the phase-matching conditions between Ar and N_2 should also be similar. From comparison of the resonance phenomena in Figs. 5 and 6, it may be concluded that the differences in the behavior of Ar and N_2 is unlikely to originate from phase-matching effects.

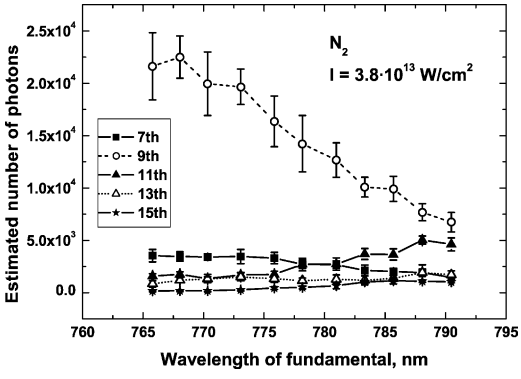

Fig. 6. Harmonic yield dependence on fundamental wavelength for N_2. Laser intensity in the focus was kept constant 3.8×10^{13} W/cm^2.

The increase of intensity in the 15th harmonic order with longer fundamental wavelengths in Ar, witnessed in Fig. 5, follows directly from the cut-off law of HHG, Eq. (1), where $U_p \propto \lambda^2$. Thus, longer wavelength radiation generates higher harmonic orders. The lower ionization potential of Kr (13.94 eV) causes the cut-off position to be at longer wavelengths than for Ar, thus a similar behavior is present for the 13th harmonic in Kr. The cut-off dependence on intensity is seen in Fig. 3 where close-to-cut-off harmonics do not saturate with intensity while plateau harmonics do.

The number of photons generated per plateau-harmonic is almost an order of magnitude higher in Kr than for corresponding harmonics in Ar. This is not surprising, since Kr is more strongly polarizable then Ar, simply in view of the larger number of electrons. However, higher orders and shorter wavelengths can be achieved with Ar; this is associated with the higher ionization potential and saturation intensity. Static average polarizabilities for Ar and N_2 are alike (1.6 and 1.7 $\times 10^{-24}$ cm^3, respectively). Nevertheless, harmonic conversion efficiencies for Ar are higher then for N_2, which is in good agreement with the results presented in Ref. [14].

The bandwidth characteristics of the generated high-order harmonics were investigated by performing absorption spectroscopy on accurately known atomic resonance lines. Absorption spectra in the XUV were recorded by scanning the cw Ti:Sapphire ring-laser, with online monitoring of frequency by a calibrated wavelength meter (Atos). The observed widths in the recording of spectral lines (Fig. 8) are convolutions of XUV harmonic bandwidth, Doppler broadening and natural line-width of the atomic transition. By neglecting the later and deconvoluting the estimated

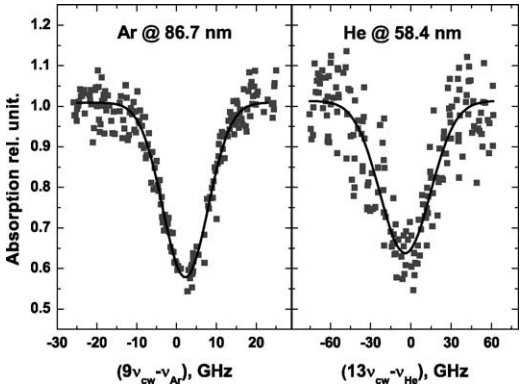

Fig. 8. High-order harmonic spectra: on the left spectral absorption recording of the ($3p^6\,{}^1S_0 \rightarrow 3p^5 3d'[3/2]_1$) transition in Ar with the 9th harmonic generated in N_2 ($\lambda_{cw} = 780$ nm); on the right spectral absorption recording of the ($1s^2\,{}^1S_0 \rightarrow 1s2p\,{}^1P_1$) transition in He with the 13th harmonic generated in N_2 ($\lambda_{cw} = 759$ nm). Note that wider scan-width in He absorption is mainly caused by bigger Doppler width. The zero points on the horizontal axis correspond to the exact position of the resonances.

Doppler broadening, the XUV bandwidth is estimated at 10–15 GHz in the 40–100 nm region (for more details see Ref. [7]). This results in an unprecedented spectral purity of $\lambda/\Delta\lambda > 2.5 \times 10^5$.

4. Conclusions

In conclusion, a narrow band tunable XUV laser radiation, based of HHG, is demonstrated. An unprecedented spectral purity $\lambda/\Delta\lambda$ of 2.5×10^5 covering the entire 40–100 nm region of tunability is reached due to long (300 ps) generating pulses. Shortest wavelength radiation was generated in Ar and N_2, but Kr displayed higher conversion efficiencies. Resonance-like phenomena of harmonic yield were observed in different gases.

Acknowledgments

M.B. and A.P. acknowledge the European Union for a Marie Curie host site fellowship at LCVU (HPMT-CT-2000-00063). This study is supported by the European Community—Integrated Infrastructure Initiative action (RII3-CT-2003-506350). D.N. acknowledges the financial support of the Australian Research Council and Centre for Ultrahigh-bandwidth Devices for Optical Systems (CUDOS).

References

[1] E. Seres, J. Seres, F. Krausz, C. Spielmann, Phys. Rev. Lett. 92 (2004) 163002.
[2] C. Spielmann, N.H. Burnett, S. Sartania, R. Koppitsch, M. Schnurer, C. Kan, M. Lenzner, P. Wobrauschek, F. Krausz, Science 278 (1997) 661.
[3] J.C. Solem, G.C. Baldwin, Science 218 (1982) 229.
[4] K.S.E. Eikema, W. Ubachs, W. Vassen, W. Hogervorst, Phys. Rev. A 55 (1997) 1866.
[5] P. Rupper, F. Merkt, Rev. Sci. Instrum. 75 (2004) 613.
[6] C. Lyngå, F. Ossler, T. Metz, J. Larsson, Appl. Phys. B 72 (2001) 913.
[7] F. Brandi, D. Neshev, W. Ubachs, Phys. Rev. Lett. 91 (2003) 163901.
[8] F. Brandi, I. Velchev, D. Neshev, W. Hogervorst, W. Ubachs, Rev. Sci. Instrum. 74 (2003) 32.
[9] D. Neshev, I. Velchev, W. Majewski, W. Hogervorst, W. Ubachs, Appl. Phys. B 68 (1999) 671.
[10] B. Chang, P.R. Bolton, D.N. Fittinghoff, Phys. Rev. A 47 (1993) 4193.
[11] P.B. Corkum, Phys. Rev. Lett. 71 (1993) 1994.
[12] M. Lewenstein, P. Balcou, M.Y. Ivanov, A. L'Huillier, P.B. Corkum, Phys. Rev. A 49 (1994) 2117.
[13] J.L. Krause, K.J. Schafer, K.C. Kulander, Phys. Rev. A 68 (1992) 3535.
[14] C. Lyngå, A. L'Huillier, C.-G. Wahlström, J. Phys. B 29 (1996) 3293.